Signed Distance Function Based Surface Reconstruction of a Submerged Inland Mine Using Continuous-time SLAM

Michael Bleier [†] **André Dias** [*,**] **António Ferreira** [*]
John Pidgeon [***] **José Almeida** [*,**] **Eduardo Silva** [*,**]
Klaus Schilling [+,†] **Andreas Nüchter** [+,†]

[*] *INESC Technology and Science, Porto, Portugal*
[**] *School of Engineering, Polytechnic Institute of Porto, Portugal*
[***] *BMT WBM Pty Ltd, Brisbane, Australia*
[+] *Informatics VII – Robotics and Telematics, Julius Maximilian University of Würzburg, Germany*
[†] *Zentrum für Telematik e.V., Würzburg, Germany,*
(e-mail: michael.bleier@telematik-zentrum.de)

Abstract: The planning of mining operations in water filled open-pit mines requires detailed bathymetry to create a mine plan and assess the involved risks. This paper presents post-processing techniques for creating an improved 3D model from a survey carried out using an autonomous surface vehicle with a multibeam sonar and a GPS/INS navigation system. Inconsistencies of the created point cloud as a result of calibration errors or GPS signal loss are corrected using a continuous-time simultaneous localization and mapping (SLAM) solution. Signed distance function (SDF) based mapping is employed to fuse the measurements from multiple runs into a consistent representation and reduce sensor noise. From the signed distance function model we reconstruct a 3D surface mesh. We use this terrain model to establish a virtual reality scene for immersive data visualization of the mining operations for testing and planing during development. Results of the proposed approach are demonstrated on a dataset captured in an abandoned submerged inland mine.

Keywords: marine systems, underwater mapping, 3D reconstruction

1. INTRODUCTION

The presented work was carried out within the Horizon 2020 research project Viable Alternative Mine Operating System (¡VAMOS!). The objective of this project is the development of a prototype mining system to extract raw materials from an abandoned water-filled open-pit mine. These inland mines have been considered depleted in the past because with previous mining techniques it was not economically viable anymore to continue operations. Today, with rising prices of certain rare ores it might become interesting again to re-open these mines in order to access deeper seated minerals. However, once the mining operations stop and no water control is carried out anymore open-pit mines eventually fill up with ground or surface water. Conventional mining techniques require high treatment and dewatering costs. This is especially problematic in the presence of high pressure aquifers. Moreover, from an environmental perspective it is desirable that the water table of these flooded inland mines is not changed. Therefore, the ¡VAMOS! project aims to develop a new remotely controlled underwater mining technique, which is environmentally and economically more viable than the state-of-the-art.

A virtual reality scene of the envisioned mining system is depicted in Fig. 1. From a launch and recovery vessel a mining vehicle is lowered to the bottom of the mine pit. It is remotely controlled from a control center located on the surface via optical fiber and electrically powered by an umbilical cord. The mining vehicle cuts the ore using a hydraulic roadheader type cutter. The ore is collected by a suction mouth located below the cutter and the slurry is pumped to the surface through a vertical riser hose.

For planning these types of operations and assessing the viability of performing mining trials detailed bathymetry of potential mining sites are necessary. However, many older mines do not have detailed historic records available. Moreover, the records might not represent the current state due to backfilling or instabilities. Therefore, updated map data is necessary to asses the mine site.

The presented bathymetric survey was carried out at the Bejanca mine site near Queirã village in Portugal. Mining operations were conducted there between 1919 and 1942. The minerals of interest in the open-pit mine are tin and tungsten. After the mine was closed in 1945 the pit filled with water from the winter rains. The survey showed that there has been significant backfilling, which results in a rather shallow waterbody. The submerged mine exhibits water depths of up to 27 m and a size of 125 m × 90 m.

The dataset was recorded with an autonomous surface vehicle (ASV) equipped with a multibeam sonar, Global

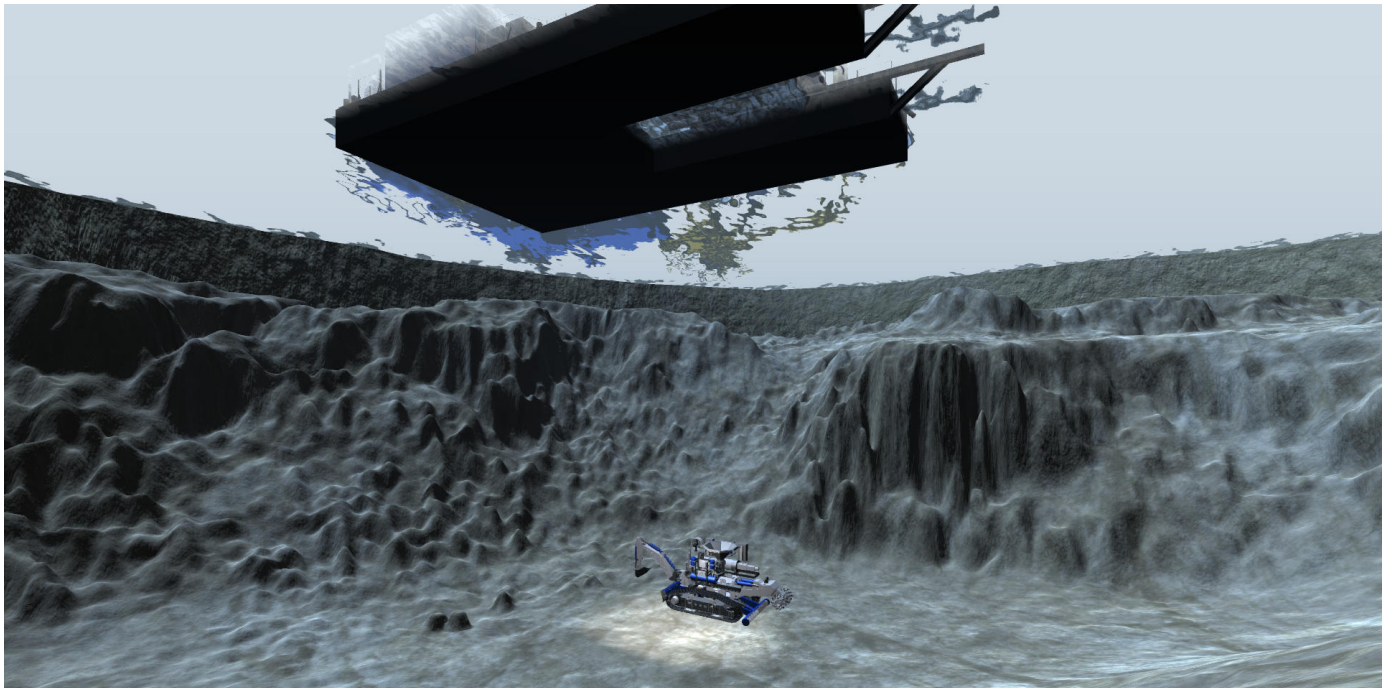

Fig. 1. Virtual reality scene of the ¡VAMOS! underwater mining system with the created terrain surface model.

Positioning System (GPS) and inertial navigation system (INS). Some errors are introduced in the multibeam survey due to inaccuracies of the vehicle motion data and calibration errors.

In this paper we propose post-processing techniques for creating a more consistent 3D mine model. The ASV took multiple passes of the mine with varying amount of overlap between individual laps, which can be exploited to compute an improved solution using a simultaneous localization and mapping (SLAM) algorithm. In this work we look at the problem of SLAM as a global trajectory optimization problem. We find an improved trajectory, such that the global consistency of point measurements is optimized. Moreover, we show how signed distance function (SDF) based mapping can be applied to fuse multiple observations into a single consistent surface representation. From the established mine model we create a virtual reality scene for immersive data visualization to find suitable landing positions for the mining vehicle, create a mine plan, or perform simulations.

2. STATE OF THE ART

Typically bathymetric maps are created with multibeam echosounders. The vehicle motion is compensated using an attitude reference system and Global Navigation Satellite System (GNSS). Nowadays, different SLAM techniques have been proposed to improve the underwater surveys.

In man-made structured environments, such as harbors, feature-based SLAM approaches have been proven to be effective. Typically employed features include planar patches (Pathak et al., 2010; Ozog and Eustice, 2013) and line features (Ribas et al., 2008).

An example of a feature-less approach is the algorithm described by Barkby et al. (2012). They use Particle Filter based SLAM to create a 2.5D point cloud of the seafloor. Individual particles are weighted based on how well the multibeam measurements agree with the global elevation map. Loop closures are detected using a Gaussian process regression of previous sonar beam observations. This allows to detect loop closures with minimal overlap and enforces consistency of neighboring map borders even if there is no overlap.

Roman and Singh (2005) divide the terrain map into smaller sub-maps that are assumed to be error free. Overlapping sub-maps are first coarsely aligned using cross correlation and then the Iterative Closest Point (ICP) algorithm is used for fine registration. The relative pose measurements are then used to further constrain an Extended Kalman Filter (EKF) based mapping procedure. Bichucher et al. (2015) extend this approach with a Graph SLAM based framework to improve the full trajectory. Palomer et al. (2016) propose a coarse-to-fine scan matching technique using ICP, which takes point measurement uncertainties into account during submap registration. The proposed approach in this paper differs from these methods in the sense that it does not partition the trajectory into submaps, which are matched using rigid registration, but employs a continuous-time SLAM algorithm.

For many bathymetry application 2.5D digital elevation maps (DEM) are created. More recently creating dense surface models from sonar imaging has become of interest. However, the significant amount of noise in acoustic measurements makes it challenging to extract surface meshes directly from the point cloud. Therefore, for reconstructing meshes from noisy data often the point measurements are integrated into an implicit surface description (Hornung and Kobbelt, 2006) or robust local surface descriptors are fitted to the 3D point cloud (Campos et al., 2014). Our work follows this direction and uses an SDF voxel map as an intermediate implicit surface model to create a more noise free representation.

3. MULTIBEAM SONAR SURVEY OF A SUBMERGED INLAND MINE

The robotic boat used for the mine mapping is the ASV ROAZ (Ferreira et al., 2009). It is a 4m long twin hull robotic vehicle with electric propulsion and autonomous navigation and control, see Fig. 2. For bathymetric mapping it is equipped with an Imagenex Delta T multibeam profiling sonar, which has a fan angle of 120 deg and a maximum range of 100 m. The experiments were conducted with a resolution of 480 beams and a beam width of 1.5 deg. Sonar data was recorded at 10 Hz.

For positioning and localization of the vehicle a L1/L2 precision GPS unit with Real Time Kinematic (RTK) differential corrections and a fiber optic based INS were installed on the robotic boat. The employed fiber optic gyro features a very low drift rating of only 0.05 deg /h. A high precision localization solution is later obtained by post-processing the raw INS data in combination with the raw GPS data. The post-processing step is performed using the Inertial Explorer software (NovAtel, 2016), where all raw GPS observations are processed in RTK and integrated with raw inertial measurements in a tightly coupled manner.

The multibeam sonar, GPS antenna and INS were mounted rigidly to the same sensor bar. This was done to ensure that the relative positions and orientations stay consistent even during transport, which requires some disassembly. The sensor bar was mounted to the front of the vehicle with the multibeam sonar only a few centimeters below the water surface. The translation offsets between the individual sensors were measured manually. Rotational offsets between the INS and multibeam sonar are later estimated using a calibration routine as described in Sec 4.1. All sensor measurements are recorded with GPS timestamps for correct data association.

The use of an ASV with autonomous navigation and synchronized on board logging capabilities allowed for an efficient data acquisition process. A trajectory was chosen, such that there is about 30 - 50% overlap between individual laps of the surface vehicle and all parts of the mine are covered multiple times.

Fig. 2. ROAZ surface vehicle at the Bejanca mine site.

4. 3D MINE MAPPING AND MULTIPLE-VIEW DATA INTEGRATION

For integrating measurements from multiple passes with the multibeam sonar we choose to employ SDF-based mapping. SDF voxel maps represent the surfaces implicitly by storing in each voxel cell the signed distance to the closest surface. Typically, the signed distance is only stored in a narrow band around the surfaces, which is referred to as a truncated signed distance function (TSDF). This representation became popular in the robotic mapping community with the work of Newcombe et al. (2011) on KinectFusion, which demonstrated excellent real time 3D reconstruction and tracking results.

A SDF map is a beneficial surface representation because noisy measurements are smoothed over multiple observations. However, overlap errors between multiple laps of the multibeam survey due to inaccuracies of the vehicle trajectory measurement or calibration errors can result in errors of the SDF model. In this case individual scan segments might not line up very well, which creates artifacts in the resulting surface model, such as additional surfaces or gaps in the 3D reconstruction. Therefore, we first apply a continuous-time SLAM technique to compute an improved trajectory of the robotic vehicle, which optimizes point cloud consistency. The examples shown in this paper are specific to a multibeam sonar, and the surface vehicle does not perform fully unconstrained 6-DOF motion. Please note that the proposed approach generalizes well to other types of sensors and unrestricted motion.

4.1 Calibration

Although great care was taken to mount the INS and multibeam sonar aligned to the sensor bar, we need to calibrate the rotational offset between the two reference systems. Even very small alignment errors introduce large inconsistencies in the resulting point cloud. To do this we manually select a short trajectory segment, which we can assume to have minimal drift. Then the rotational offset is optimized based on an error measurement which determines point cloud quality similar to Sheehan et al. (2012). The error measurement is computed by splitting the trajectory into overlapping parts and calculating a point distance error based on closest point correspondences. We find the rotational offset parameters that minimize the error and verify the result on different trajectory segments.

4.2 Continous-time SLAM

For processing the multibeam sonar data, we employ a continuous-time SLAM solution, also called semi-rigid SLAM. To understand the basic idea, we summarize its basis, 6D SLAM, which was initially designed as a Graph-SLAM solution for point clouds. 6D SLAM works similarly to the the well-known ICP algorithm, which minimizes the following error function

$$E(\mathbf{R},\mathbf{t}) = \frac{1}{N}\sum_{i=1}^{N} \left\| \mathbf{m}_i - (\mathbf{R}\mathbf{d}_i + \mathbf{t}) \right\|^2 \qquad (1)$$

to solve iteratively for an optimal transformation $\mathbf{T} = (\mathbf{R},\mathbf{t})$ with rotation $\mathbf{R}$ and translation $\mathbf{t}$, where the tuples

$(\mathbf{m}_i, \mathbf{d}_i)$ of corresponding model $\mathbf{M}$ and data points $\mathbf{D}$ are given by minimal distance, i.e., $\mathbf{m}_i$ is the closest point to $\mathbf{d}_i$ within a close limit (Besl and McKay, 1992). Instead of the two-scan-Eq. (1), we look at the n-scan case:

$$E = \sum_{j \to k} \sum_{i} \left| \mathbf{R}_j \mathbf{m}_i + \mathbf{t}_j - (\mathbf{R}_k \mathbf{d}_i + \mathbf{t}_k) \right|^2 , \qquad (2)$$

where j and k refer to scans of the SLAM graph, i.e., to the graph modelling the pose constraints in SLAM. If they overlap, i.e., closest points are available, then the point pairs for the link are included in the minimization. We solve for all poses at the same time and iterate like in the original ICP. The derivation of a GraphSLAM method using a Mahalanobis distance that describes the global error of all the poses

$$W = \sum_{j \to k} (\bar{\mathbf{E}}_{j,k} - \mathbf{E}'_{j,k})^T \mathbf{C}^{-1}_{j,k} (\bar{\mathbf{E}}'_{j,k} - \mathbf{E}'_{j,k}) \qquad (3)$$

where $\mathbf{E}'_{j,k}$ is the linearized error metric and the Gaussian distribution is $(\bar{\mathbf{E}}_{j,k}, \mathbf{C}_{j,k})$ with computed covariances from scan matching as given in Borrmann et al. (2008) does not lead to different results. Please note, while there are four closed-form solutions for the original ICP Eq. (1), linearization of the rotation in Eq. (2) or (3) is always required.

Semi-rigid SLAM. The algorithm is adopted from Elseberg et al. (2013), where it was used in different mobile mapping contexts. We make no rigidity assumptions, except for the computation of the point correspondences. We also require no explicit motion model. This means the specific dynamics of the employed vehicle do not need to be known. The continuous-time SLAM for trajectory optimization works in full 6 DoF. The algorithm requires no computation of high-level visual or geometric feature descriptors, i.e., we require only the points themselves.

In case of multibeam sonar mapping, we do not have separate 3D point clouds, just slices. In the current state of the art developed by Bosse and Zlot (2009) for improving overall map quality of mobile mappers in the robotics community the time is coarsely discretized. This results in a partition of the trajectory into sub-scans that are treated rigidly. Then rigid registration algorithms like the ICP and other solutions to the SLAM problem are employed. Obviously, trajectory errors within a sub-scan cannot be improved in this fashion. Applying rigid pose estimation to this non-rigid problem directly is also problematic since rigid transformations can only approximate the underlying ground truth. When a finer discretization is used, single 2D scan slices or single points result that do not constrain a 6 DoF pose sufficiently for rigid algorithms.

Mathematical details of our algorithm are given in Elseberg et al. (2013). Essentially, we first split the trajectory into sections, and match these sections using the automatic high-precise registration of terrestrial 3D scans, i.e., globally consistent scan matching (Borrmann et al., 2008). Here, the graph is estimated using a heuristics that measures the overlap of sections using the number of closest point pairs. After applying globally consistent scan matching on the sections the actual semi-rigid matching as described in Elseberg et al. (2013) is applied, using the results of the rigid optimization as starting values to compute the numerical minimum of the underlying least square problem. To speed up the calculations, we make use of the sparse Cholesky decomposition.

A key issue in continuous-time SLAM is the search for closest point pairs. We use an octree and a multi-core implementation using OpenMP to solve this task efficiently. A time-threshold for the point pairs is used, i.e., we match only to points, if they were recorded at least t_d time steps away. For the presented experiments we choose a duration of 30 s which corresponds to 300 sonar scan slices. In addition, we use a maximal allowed point-to-point-distance which has been set to 50 cm.

4.3 Signed Distance Function Based Mapping

We integrate all sonar scans into a SDF voxel model based on the optimized trajectory computed by the continuous-time SLAM solution. The signed distance measurement $d(\mathbf{v})$ for a voxel with center $\mathbf{v}$ is computed as follows

$$d(\mathbf{v}) = m - \left\| \mathbf{p} - \mathbf{v} \right\| , \qquad (4)$$

where $\mathbf{p}$ is the sensor position and m is the distance measurement of the sensor. Multiple measurements of the same voxel cell are integrated based on a weighting function f. This way noise cancels out over multiple observations. We store in each voxel cell the signed distance $s(\mathbf{v})$ and the weight $w(\mathbf{v})$. To integrate a new measurement $d(\mathbf{v})$ at iteration $k+1$ we compute the weighted average

$$s_{k+1}(\mathbf{v}) = \frac{w_k(\mathbf{v}) s_k(\mathbf{v}) + f d_{k+1}(\mathbf{v})}{w_k(\mathbf{v}) + f} , \qquad (5)$$

where f is a weight assigned to the new measurement. The signed distance is truncated to the interval $[s_{\min}; s_{\max}]$. Since we do not have an accurate noise model of the sonar sensor uniform weights ($f = 1$) are employed. The weight is updated by

$$w_{k+1}(\mathbf{v}) = \min(w_k(\mathbf{v}) + f, w_{\max}) , \qquad (6)$$

where $w_{\max}$ is the maximum weight. For the experiments in this paper we choose $w_{\max} = 20$.

SDF-based mapping is not completely robust to coarse outliers. Noisy surfaces are only smoothed if the individual measurements lie within a certain band, which is determined by the penetration depths $D_{\min}$ and $D_{\max}$ of the TSDF. Underwater sonar sensors typically exhibit some amount of coarse outliers. Measurement points that lie outside the truncation thresholds are integrated as additional surfaces. To address this problem we choose a large truncation threshold of 1.5 m. This limits the minimum thickness of objects that can be represented by the SDF model. However, in the particular case of the submerged inland mine this is not an issue because we only want to represent a single surface of the mine floor. To remove erroneous integrated surfaces we filter the SDF voxels based on the weight. This is based on the assumption that voxels representing real surfaces carry a higher weight, i.e., are observed more often, compared to voxels filled from measurement outliers.

For modeling the mine we choose a voxel resolution of 10 cm. This means the TSDF space of the entire mine has a size in the order of a billion voxels. In order to store large maps with low memory consumption we need to encode free space efficiently. Different techniques to do this have been proposed: Whelan et al. (2012) store a

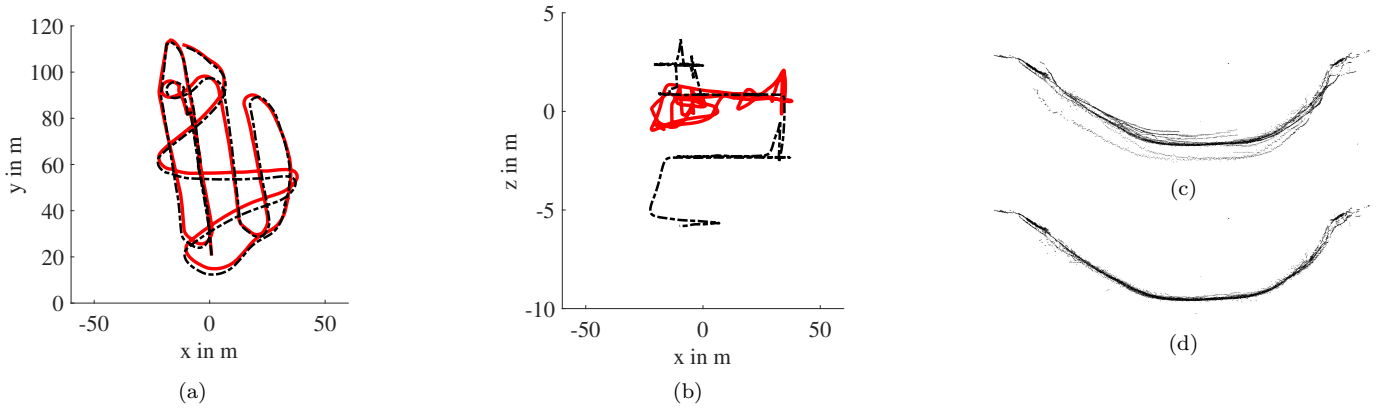

Fig. 3. Initial (black dashed line) and optimized (red line) trajectory (a,b), and cross sections of the point clouds created using the initial GPS/INS (c) and optimized trajectory (d).

dense representation of the TSDF dynamically in a small predefined volume around the sensor in motion. The parts of the map that move outside this volume are converted to a triangular mesh and only the mesh is stored. Methods for storing the entire TSDF are voxel hashing (Nießner et al., 2013) or octree data structures (Steinbrücker et al., 2014). For this work we use a B-tree based data structure (Museth, 2013) to store the complete sparse TSDF grid. The tree has constant depth, which allows constant time local and random traversals. We use a three-level tree with branching factors decreasing closer to the leaves.

To integrate the multibeam data in the TSDF we follow the generalized sensor fusion approach proposed by May et al. (2014). We model the multibeam as a polar line sensor with a beam width of 1.5 deg. Individual voxel cells within measurement range are then updated based on back projection using this sensor model. From the scalar TSDF grid we finally extract a surface mesh for visualization using the marching cubes algorithm.

4.4 Results

To demonstrate the continuous-time SLAM algorithm Fig. 3 shows results on a trajectory with significant drift of multiple meters. In this specific case the GPS signal was lost temporarily during data acquisition, which explains the large trajectory errors. The dataset consists of 7291 multibeam scans captured at 10 Hz. It was captured in 13 min and the trajectory is 757 m long (result of the SLAM solution). Fig. 3 (a,b) depict the initial GPS/INS trajectory as a black dashed line and the optimized trajectory as a red continuous line. The x/y-plane is aligned parallel to the water surface. We can see that SLAM converges to a solution that puts the sensor poses closer to a planar motion as expected for a surface vehicle. Please note that the algorithm does not impose any movement constraints or rely on a vehicle motion model. Cross sections of the resulting point cloud are displayed in Fig.3 (c,d). We can clearly see misalignment between multiple passes of the multibeam sonar in the initial result shown in Fig.3 (c). Point measurements line up well using the improved trajectory estimate based on continuous-time SLAM visualized in Fig.3 (d).

Moreover, also data captured with a good GPS/INS result can be further improved using the proposed techniques as depicted in Fig. 4. Fig. 4(a) shows the resulting point cloud using the GPS/INS trajectory while Fig. 4(b) shows the result using the optimized trajectory from continuous-time SLAM. The color encodes the depth. This dataset consists of 12786 multibeam scans captured at 10 Hz. It was captured in 22 min and the trajectory is 1567 m long (result of the SLAM solution). Especially at the bottom of the mine it is visible that the multibeam measurements are more consistent in the optimized results. This can be seen more clearly in the cross sections of the point clouds presented in Fig. 4(e) and Fig. 4(f).

Consequently, the extracted mesh from the SDF representation using the optimized continuous-time SLAM solution, depicted in Fig. 4(d), exhibits smoother surfaces than the initial result depicted in Fig. 4(c). Despite the noise of the measurements a smooth surface can be extracted if a sufficient amount of repeated observations are available.

The borders of the mine show holes in the mesh. This is a result of the irregular and low point density of the sonar measurements due to limited coverage close to the borders of the mine. Since this is undesirable, we later interpolate the holes for display in the virtual reality system.

5. CONCLUSION

In this paper we showed first results on creating a detailed terrain model of a submerged inland mine from a multibeam sonar survey. We demonstrate that SLAM techniques are effective to remove inconsistencies due to inaccuracies of the motion data. Moreover, we presented a signed distance function based approach for data fusion.

Rendering a surface mesh for visualization compared to a point cloud is advantageous because it allows the human operator to see the surfaces and structure more clearly. We integrate the terrain model into a virtual reality scene together with prototype models of the envisioned mining system, which is used for pre-planning, visualization and development.

ACKNOWLEDGEMENTS

This work was supported by the European Union's Horizon 2020 research and innovation programme under grant agreement No 642477.

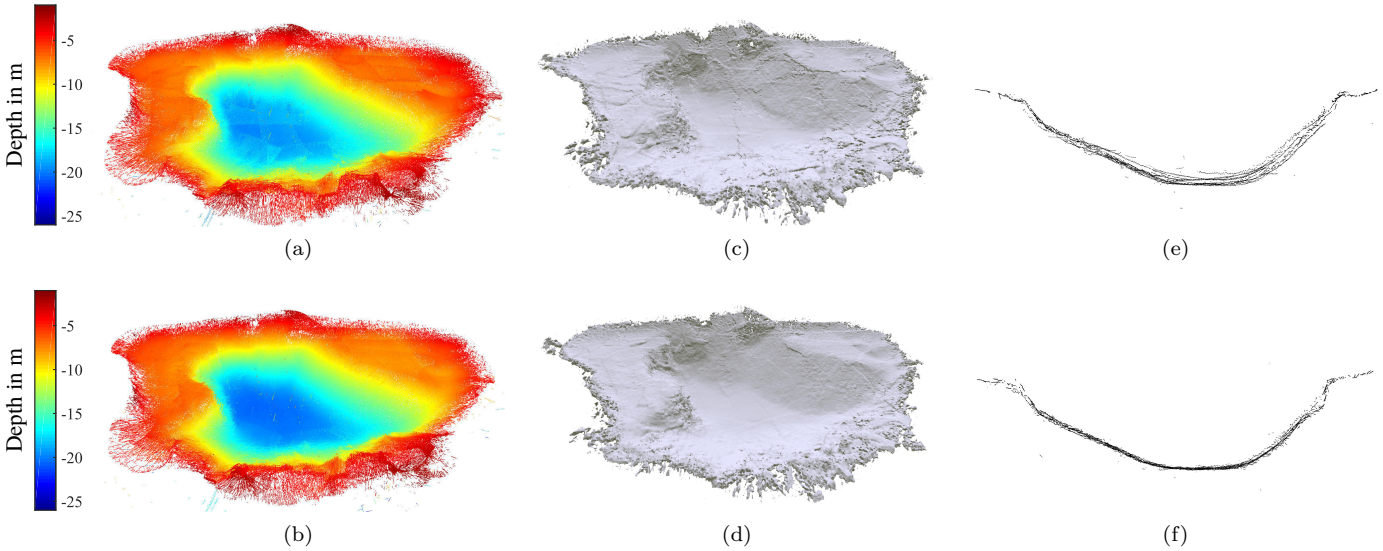

Fig. 4. Initial (a) and optimized (b) 3D point cloud, surface mesh extracted from SDF model using initial GPS/INS (c) and continuous-time SLAM solution (d), and a cross section of initial (e) and optimized (f) point cloud.

REFERENCES

Barkby, S., Williams, S.B., Pizarro, O., and Jakuba, M.V. (2012). Bathymetric particle filter SLAM using trajectory maps. *The International Journal of Robotics Research*, 31(12), 1409–1430.

Besl, P.J. and McKay, N.D. (1992). Method for registration of 3-D shapes. In *IEEE Trans. Pattern Analysis and Machine Intelligenc*, volume 14, 239–256.

Bichucher, V., Walls, J.M., Ozog, P., Skinner, K.A., and Eustice, R.M. (2015). Bathymetric factor graph SLAM with sparse point cloud alignment. In *Proc. OCEANS 2015 - MTS/IEEE Washington*, 1–7.

Borrmann, D., Elseberg, J., Lingemann, K., Nüchter, A., and Hertzberg, J. (2008). Globally consistent 3D mapping with scan matching. *Robotics and Autonomous Systems*, 56(2), 130–142.

Bosse, M. and Zlot, R. (2009). Continuous 3D scan-matching with a spinning 2D laser. In *Proc. IEEE Int. Conf. Robotics and Automation*, 4312–4319.

Campos, R., Garcia, R., Alliez, P., and Yvinec, M. (2014). A surface reconstruction method for in-detail underwater 3D optical mapping. *The International Journal of Robotics Research*, 64 – 89.

Elseberg, J., Borrmann, D., and Nüchter, A. (2013). Algorithmic solutions for computing precise maximum likelihood 3D point clouds from mobile laser scanning platforms. *Remote Sensing*, 5(11), 5871–5906.

Ferreira, H., Almeida, C., Martins, A., Almeida, J., Dias, N., Dias, A., and Silva, E. (2009). Autonomous bathymetry for risk assessment with ROAZ robotic surface vehicle. In *Proc. OCEANS 2009 - Europe*, 1–6.

Hornung, A. and Kobbelt, L. (2006). Robust reconstruction of watertight 3D models from non-uniformly sampled point clouds without normal information. In *Fourth Eurographics Symp. on Geometry Processing*, 41–50.

May, S., Koch, P., Koch, R., Merkl, C., Pfitzner, C., and Nüchter, A. (2014). A generalized 2D and 3D multi-sensor data integration approach based on signed distance functions for multi-modal robotic mapping. In *19th Int. Workshop on Vision, Modeling and Visualization*, 95–102.

Museth, K. (2013). VDB: High-resolution sparse volumes with dynamic topology. *ACM Transactions on Graphics*, 32(3), 27.

Newcombe, R.A., Izadi, S., Hilliges, O., Molyneaux, D., Kim, D., Davison, A.J., Kohi, P., Shotton, J., Hodges, S., and Fitzgibbon, A. (2011). KinectFusion: Real-time dense surface mapping and tracking. In *Proc. 10th IEEE Int. Mixed and Augmented Reality Symp.*, 127–136.

Nießner, M., Zollhöfer, M., Izadi, S., and Stamminger, M. (2013). Real-time 3D reconstruction at scale using voxel hashing. *ACM Transactions on Graphics*, 32(6), 169.

NovAtel (2016). Inertial Explorer. `http://www.novatel.com/products/software/inertial-explorer/`.

Ozog, P. and Eustice, R.M. (2013). Real-time SLAM with piecewise-planar surface models and sparse 3D point clouds. In *Proc. IEEE/RSJ Int. Conf. Intelligent Robots and Systems*, 1042–1049.

Palomer, A., Ridao, P., and Ribas, D. (2016). Multibeam 3D underwater slam with probabilistic registration. *Sensors*, 16(4), 560.

Pathak, K., Birk, A., and Vaskevicius, N. (2010). Plane-based registration of sonar data for underwater 3D mapping. In *Proc. IEEE/RSJ Int. Conf. Intelligent Robots and Systems*, 4880–4885.

Ribas, D., Ridao, P., Tardós, J.D., and Neira, J. (2008). Underwater SLAM in man-made structured environments. *Journal of Field Robotics*, 25(11-12), 898–921.

Roman, C. and Singh, H. (2005). Improved vehicle based multibeam bathymetry using sub-maps and SLAM. In *Proc. IEEE/RSJ Int. Conf. Intelligent Robots and Systems*, 3662–3669.

Sheehan, M., Harrison, A., and Newman, P. (2012). Self-calibration for a 3D laser. *The International Journal of Robotics Research*, 31(5), 675–687.

Steinbrücker, F., Sturm, J., and Cremers, D. (2014). Volumetric 3D mapping in real-time on a CPU. In *Proc. IEEE Int. Conf. Robotics and Automation*, 2021–2028.

Whelan, T., Kaess, M., Fallon, M., Johannsson, H., Leonard, J., and McDonald, J. (2012). Kintinuous: Spatially extended KinectFusion. Technical report, Massachusetts Institute of Technology.